Exp Astron (2017) 44:287–296
DOI 10.1007/s10686-017-9548-z

An XMM-Newton proton response matrix

Teresa Mineo[1] · Simone Lotti[2] · Silvano Molendi[3] · Simona Ghizzardi[3]

Received: 19 January 2017 / Accepted: 6 July 2017 / Published online: 5 August 2017

Abstract Soft protons constitute an important source of background in focusing X-ray telescopes, as Chandra and XMM-Newton experience has shown. The optics in fact transmit them to the focal plane with efficiency similar to the X-ray photon one. This effect is a good opportunity to study the environment of the Earth magnetosphere crossed by the X-ray satellite orbits, provided that we can link the spectra detected by the instruments with the ones impacting on the optics. For X-ray photons this link has the form of the so-called response matrix that includes the optics effective area and the energy redistribution in the detectors. Here we present a first attempt to produce a proton response matrix exploiting ray-tracing and GEANT4 simulations with the final aim to be able to analyse XMM-Newton soft proton data and link them to the external environment. If the procedure is found to be reliable, it can be applied to any future X-ray missions to predict the soft particles spectra impacting on the focal plane instruments.

Keywords Background radiation · X-ray telescopes and instruments · X-ray

✉ Teresa Mineo
mineo@iasf-palermo.inaf.it

[1] INAF-IASF Palermo, via U. La Malfa 153, 90146 Palermo, Italy

[2] INAF-IAPS, via del Fosso del Cavaliere 100, 00113 Roma, Italy

[3] INAF-IASF Milano, Via E. Bassini 15, 20133 Milano, Italy

1 Introduction

The X-ray telescope capability of focusing protons with energies lower that a few hundred keV was discovered just after *Chandra* X-ray observatory [17] launch, when a rapid degradation of the front illuminated CCDs at the focal plane of the Wolter 1 telescope occurred [14]. The damages were caused by protons populating the radiation belts of the Earth magnetosphere crossed by the telescope during the perigee passage. XMM-Newton [12] is exposed to the same risks being operated in a similar orbit but, in this case, instruments have been protected since the mission's start by closing the filter wheel during the perigee passage and switching-off the detectors in case of intense solar activity. Unfortunately, soft proton contamination is observed also out of the radiation belts in form of flaring events during which the background rate can reach up to thousand times the quiescent level. These flares affect about 30–40% of the observing time and can last from hundreds of seconds to hours.

However, even if this effect degrades the telescope performances in observing X-ray sources, it could be a good opportunity to study the environment of the Earth magnetosphere crossed by the satellite orbits. The key in using the X-ray telescope as proton telescope is the capability in linking the spectra detected by the instruments with the ones impacting on the optics. This is possible by correctly modelling the physical processes involved in the interactions with all elements of the telescope.

In the standard X-ray data analysis the spectrum emitted by the observed source is derived from the detected one using XSPEC [9]. This is an interactive X-ray spectral-fitting program opportunely designed to be detector-independent. The specific characteristics of instruments are introduced with a response matrix.

In this paper, we present the simulations used to build a first version of the protons response matrix for the Metal Oxide Semi-conductor (MOS) CCDs at the focal plane of XMM-Newton and a simple test on its validity, together with a discussion on some critical points still present in the procedure.

2 Physics interactions

XMM-Newton carries three X-ray telescopes each composed by 58 Wolter I grazing-incidence mirrors nested in a coaxial and cofocal configuration. The mirror shells have very shallow grazing angles ($\sim 30'$) in order to reflect photons up to 10 keV. Each telescope includes a baffle for visible and X-ray stray-light suppression. The detector at the focal plane, the European Photon Imaging Camera (EPIC), consists on three CCD cameras: two MOS and one pn CCD array.

The MOS camera is an array of front illuminated CCDs with a sensitive depth of 40 μm of silicon. The electrodes of the pixels have a complex structure: about 40% of their area (open electrode) is covered by a layer of 0.1 μm silicon and 0.15 μm silicon dioxide, while the other 60% (normal electrode) has a thickness of 0.3 μm silicon and 0.75 μm silicon dioxide. The MOS telescopes are equipped with Reflection Grating Spectrometers (RGS) that intercept about half of the X-ray light deflecting it to an off-set detector; photons reaching the MOS area ($28.4'$ diameter) are then 50% of the collected ones.

EPIC detectors are protected from the background induced by IR, visible and UV light with three different optical blocking filters mounted on a filter wheel that can be exchanged depending on the requirement on the observations: the thin filter is made of 1600 Å polyimide film with 400 Å of aluminium evaporated on one side; the medium filter has 800 Å of aluminium deposited on the same material as the thin filter; and 1100 Å of aluminium and 450 Å of tin are evaporated on a 3300 Å polypropylene film for the thick filter.

The interaction of protons with each single elements of the telescope is driven by different phenomena mainly because of the incident angles involved: the optics reflect protons coming at grazing incident angles, while the filter and the CCDs receive protons with almost normal directions.

The model for the proton interaction with the coated surface of the optics adopted in the production of the response matrix was derived by Remizovich et al. [16] solving the transport equation for glancing incident ion beams in the diffusion approximation. The final general formula for the reflection probability in a given direction per unit surface and unit area (Eq. 33 in [16]) assumes a simplified form (Eq. 37 in [16]) under the assumption of almost elastic reflection. In this case, the scattering distribution for a beam incidents at polar angle ϑ_{in} and zero azimuthal angle is given by the following formula normalized to unity and expressed in term of the polar and azimuthal dimensionless variables ψ and ξ:

$$W(\psi, \xi) = \frac{1}{12\,\pi\,\psi^{1/2}} \left[\frac{\omega^4}{1+\omega^2} + \omega^3 \arctan \omega \right] \tag{1}$$

with

$$\omega = \left\{ \frac{3\,\psi}{\psi^2 - \psi + 1 + (\xi/2)^2} \right\}^{1/2} \tag{2}$$

where ψ is the output polar angle normalized to the incident angle ($\psi = \vartheta_{out}/\vartheta_{in}$) and ξ the output azimuthal angle normalized to the polar incident angle ($\xi = \phi_{out}/\vartheta_{in}$). This scattering probability $W(\psi, \xi)$ is defined as the ratio of the rate of particles reflected in a given direction from a unit area to the rate of particles incident on the same area. Integrating (1) over ξ, the formula for the polar distribution published by Firsov [10] is obtained:

$$W(\psi) = \frac{3}{2\,\pi} \frac{\psi^{3/2}}{1+\psi^3} \tag{3}$$

Plots relative to the adopted reflection function are shown in Fig. 1. In particular, the top panel shows the polar distribution (3) as function of the dimensionless variable ψ. In the bottom panel, the azimuthal distributions (1) as function of the dimensionless variable ξ is shown for $\psi = 0.3$ (magenta), $\psi = 1$ (blue) and $\psi = 3.0$ (green). The three curves are normalised to their maximum to highlight that the width of the distribution increases at larger polar angles. These plots clearly show that the maximum scattering probability is obtained at output angles equal to the input ones.

The interactions with the filters and the CCD are treated through the stopping power, that is the energy loss due to Coulomb excitation and ionizations of the

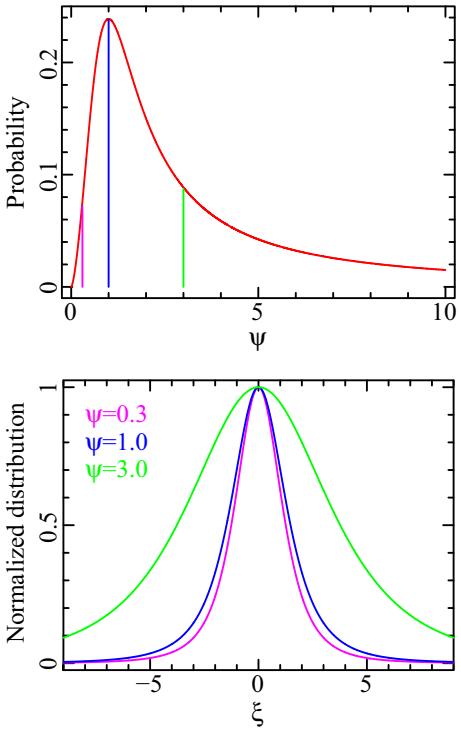

Fig. 1 Probability distribution for the proton scattering angles after the interaction with the optics. *Top panel:* Polar distribution integrated over the azimuthal angles as function of the dimensionless variable ψ. The *vertical lines* indicate the values of ψ used to compute the azimuthal distributions in the bottom panel. *Bottom panel:* Azimuthal distribution normalized to one as function of the dimensionless variable ξ for $\psi = 0.3$ (*magenta*), $\psi = 1$ (*blue*) and $\psi = 3.0$ (*green*). The proper integral of the *curves* is 0.08 for $\psi = 0.3$, 0.24 for $\psi = 1$ and 0.09 for $\psi = 3.0$

electrons in the medium, derived within the Bethe theory [4]. The processes are treated with Monte Carlo methods using GEANT4 [1–3] a toolkit that includes a full set of models for the interaction of protons. A validation for GEANT4 applicability in simulating the effects of proton induced radiation for space mission has been presented by Ivanchenko et al. [11] using available experimental data.

3 The simulation codes

The optics transmission was obtained with a ray-tracing Monte Carlo stand-alone code able to simulate either photons or protons. The code was obtained adding the proton reflection model of (1) to an existing version already used for the on-ground and in-flight calibration of the photon effective area of the X-ray telescopes*Beppo*SAX [5] and Swift [6]. It follows the particle from the interaction with the mirror shells up to the focal plane taking into account the geometry of the optics, the effects of the baffle. No reflection from the uncoated back surface of the shells is considered in this version of the code that, considering the adopted reflection model, underestimates the transmission by a factor independent on energy. Following versions of the software will take into account all possible reflections.

Protons with incident angles within the field of view of the telescope can reach the focal plane after the interaction with the two mirror sections (double reflection).

However, the focal plane can also be reached from angles out of the field of view after a single interaction with only one of the section of the mirror shells. The rate of these events is strongly limited by the presence of the baffle, but their contribution cannot be neglected. The parameter that better describe the optics transmission is the grasp $G(\vartheta, E)$ defined as:

$$G(\vartheta, E) = 2\pi \int_0^{\vartheta_{max}} A(\vartheta, E)\ \sin\vartheta\ d\vartheta \tag{4}$$

where E is the energy, $A(\vartheta, E)$ the effective area at the incident angle ϑ and $[2\pi\ \sin\vartheta\ d\vartheta]$ is the differential solid angle integrated up to the maximum off-axis angle ϑ_{max}.

We assumed a collecting radius at the focal plane of 3.25 cm, correspondent to 15′, and simulated protons up to $\vartheta = 10°$. The grasp has a maximum value of 0.015 cm^2 sr as shown in Fig. 2 where it is plotted as function of the off-axis angles. It is independent of the proton energy because the adopted reflection model is obtained in elastic approximation. A further reduction of 50% was included in the effective area to take into account the obscuration due to the gratings.

The medium filter plus the electrode transmission was computed with Monte Carlo methods using a GEANT4 code. As an estimate, a 50 keV proton loses on average 30 keV of its energy crossing the filter and other 15 keV in the open electrode. It has not sufficient energy to pass over the normal electrode were at least 100 keV are necessary for a detection. The transmission efficiency accounts only for events that deposit in the detector sensitive area an energy in the range 0.2–10 keV. The plot in Fig. 3 gives the total transmission probability as function of the input proton energy. The two peaks are due to the structure of the MOS electrode. The peak with a maximum at ∼50 keV is due to protons that interact in the thinner section of the open electrode, while the higher energy peak is produced by protons impacting on the normal electrode.

The GEANT4 code is also used to obtain, for each input energy, the spectrum of the energies deposited in the MOS after crossing the filter and the electrodes necessary for building the redistribution matrix (see Section 4).

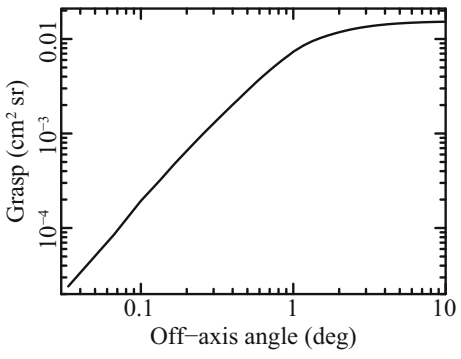

Fig. 2 XMM-Newton optics grasp as function of the off-axis angles computed with the ray-tracing

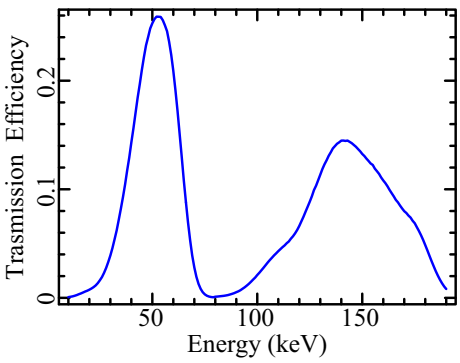

Fig. 3 Total transmission efficiency relative to the medium filter as function of the input proton energy. It accounts for the filter, the MOS electrode and the factor for the fraction of events that are detected in the energy range 0.2–10 keV

4 The MOS proton response matrix

The response matrix for the standard X-ray analysis contains the probability that an incoming photon of energy E is detected in the output detector channel PHA. To be used within XSPEC, the response matrix must be opportunely written in units of cm^2. The file, as the Office of Guest Investigators Program (OGIP) established for high-energy astrophysics projects, has a Flexible Image Transport System (FITS) format conform to the standards given in the OGIP Calibration Memo CAL/GEN/92-002.[1]

The MOS proton response matrix was coded using the same definitions and format as for photons. It is composed of two fits files:

- the ancillary response file (arf) that is an array that stores the summed contributions of all efficiencies. In the proton case, the arf file includes as multiplicative factors the telescope grasp, the grating obscuration factor, the medium filter and the electrodes transmission efficiency and the probability that an absorbed proton is detected in the MOS working range 0.2–10 keV.
- the detector redistribution matrix file (rmf) that stores in a 2-d array (energy vs PHA channel) the probability that a proton with energy E_o is detected in the channel PHA correspondent to the energy E_d. The matrix has 180 rows each correspondent to an input proton energy in the range 10–190 keV and 256 PHA output channels uniformly distributed in the range 0.2–10 keV. All rows are normalized to one.

As an example, the redistribution matrix relative to the input proton energy of 30 keV is shown in Fig. 4: the deposited energy with the highest probability corresponds to the PHA channels of $\sim$1 keV.

5 Comparison with real data

The quiescent soft proton spectrum published by Leccardi and Molendi [13] is considered to validate and test the matrix. It is relative to MOS blank field observations

[1] http://heasarc.gsfc.nasa.gov/docs/heasarc/caldb/docs/memos/cal_gen_92_002/cal_gen_92_002.html.

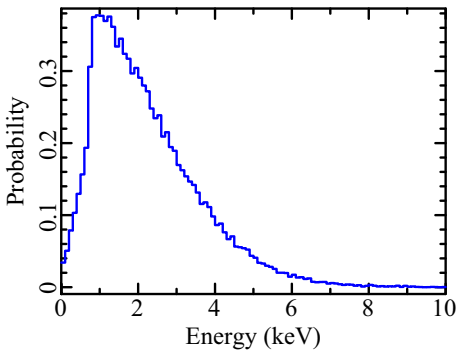

Fig. 4 Row of the redistribution matrix correspondent to the proton incident energy of 30 keV

for a total exposure of ∼600 ks and it was accumulated in the outer 10′–12′ ring of the detector. Counts in the spectrum can be modelled with a broken power law with a break energy at 5.0 keV, and the slopes fixed to 0.4 below 5 keV and 0.8 above 5 keV; the normalization at 1 keV of the MOS1 spectrum with the medium filter is $(2.6 \pm 0.1) \times 10^{-3}$ count s^{-1} keV^{-1} [13].

In order to compare this spectrum with the one obtained with our simulation, a factor due to the different selection regions is added to the transmission efficiency obtained with the simulators. In a first approximation, this factor (0.19) is simply given by the ratio between the annulus used to accumulate the spectrum (inner radius 10′; outer radius 12′) and the region assumed in the production of the matrix (a circle with 15′ radius).

Using the proton response matrix within XSPEC and assuming a simple power law as input spectrum, a flux of 420^{+234}_{-153} pr cm^{-2} s^{-1} keV^{-1} sr^{-1} and a spectral index of 1.5±0.1 were obtained, where the errors are relative to 90% confidence level. Similar values of spectral index have been measured by several authors [7, 15] during quiet intervals.

6 Critical points

This first version of a proton response matrix, even if encouraging, has several critical points that should be addressed and solved in the future versions:

– the model adopted for the reflection must be validated by experimental data. A comparison was performed with measurements performed on one of the eROSITA shells with protons at energies of 250 keV, 500 keV and 1 MeV and incidence angles between 0.3° and 1.3° [8]. The reflection model adopted in the ray-tracing reproduces the experimental results at angles $\simeq 1°$ while overestimates the efficiency at lower angles. In addition an energy loss up to maximum of 20% is observed at all energies and angles. More dedicated measurements should be compared with the available theoretical models in order to choose the one that better describes the interactions;
– being the optical blocking filter quite thin, the straggling effects and the mean energy losses as treated in GEANT4 could not have the proper precision for

modelling the transmission. Again, dedicated measurements are needed for validation;
– several proton spectra, relative to magnetosphere regions and observing periods where the input spectrum to XMM-Newton satellite is known with acceptable precision, should be used to validate the matrix.

Improvements in the modelling of the proton interactions with the telescope elements have also great importance in the framework of Athena mission to correctly evaluate the level of particle induced background. Dedicated measurements are then included in the program of two recently issued ESA tenders to test the reflection from materials as silicon or iridium that are the principal components of the Athena pore optics (EXACRAD tender) and to produce curves of proton transmission for filters with characteristics similar to the ones used in front of the two focal plane instruments X-IFU and WFI (LAOF tender).

Moreover, results from the ESA tender AREMBES produced a "space physic list" tuned for simulations of space X-ray instruments. We are then planning to use this physics list for the new versions of the matrix whose first version was produced using the *emstandard_opt4* physics list.

7 Conclusion

This first version of the soft proton response matrix indicates that it could be a powerful tool to derive the proton spectra in the magnetosphere regions crossed by the satellite. Solutions of the critical points presented in the previous section can be obtained by the several ESA tenders dedicated to validate the models of the proton interactions.

Considering that the knowledge of the orbital proton spectrum is also of great interest for the assessment of any future X-ray mission, as for example Athena, the same tool can be used to evaluate the expected rates and spectra of soft protons and to drive the design for any eventual reduction of their contamination.

Acknowledgements The results described in this paper have been reported during the AHEAD background workshop, organised with the support of the EU Horizon 2020 Programme (grant agreement n. 654215)

References

1. Agostinelli, S., Allison, J., Amako, K., Apostolakis, J., Araujo, H., Arce, P., Asai, M., Axen, D., Banerjee, S., Barrand, G., Behner, F., Bellagamba, L., Boudreau, J., Broglia, L., Brunengo, A., Burkhardt, H., Chauvie, S., Chuma, J., Chytracek, R., Cooperman, G., Cosmo, G., Degtyarenko, P., Dell'Acqua, A., Depaola, G., Dietrich, D., Enami, R., Feliciello, A., Ferguson, C., Fesefeldt, H., Folger, G., Foppiano, F., Forti, A., Garelli, S., Giani, S., Giannitrapani, R., Gibin, D., Gómez Cadenas, J.J., González, I., Gracia Abril, G., Greeniaus, G., Greiner, W., Grichine, V., Grossheim, A., Guatelli, S., Gumplinger, P., Hamatsu, R., Hashimoto, K., Hasui, H., Heikkinen, A., Howard, A., Ivanchenko, V., Johnson, A., Jones, F.W., Kallenbach, J., Kanaya, N., Kawabata, M., Kawabata, Y., Kawaguti, M.,

Kelner, S., Kent, P., Kimura, A., Kodama, T., Kokoulin, R., Kossov, M., Kurashige, H., Lamanna, E., Lampén, T., Lara, V., Lefebure, V., Lei, F., Liendl, M., Lockman, W., Longo, F., Magni, S., Maire, M., Medernach, E., Minamimoto, K., Mora de Freitas, P., Morita, Y., Murakami, K., Nagamatu, M., Nartallo, R., Nieminen, P., Nishimura, T., Ohtsubo, K., Okamura, M., O'Neale, S., Oohata, Y., Paech, K., Perl, J., Pfeiffer, A., Pia, M.G., Ranjard, F., Rybin, A., Sadilov, S., Di Salvo, E., Santin, G., Sasaki, T., Savvas, N., Sawada, Y., Scherer, S., Sei, S., Sirotenko, V., Smith, D., Starkov, N., Stoecker, H., Sulkimo, J., Takahata, M., Tanaka, S., Tcherniaev, E., Safai Tehrani, E., Tropeano, M., Truscott, P., Uno, H., Urban, L., Urban, P., Verderi, M., Walkden, A., Wander, W., Weber, H., Wellisch, J.P., Wenaus, T., Williams, D.C., Wright, D., Yamada, T., Yoshida, H., Zschiesche, D.: G EANT4 Collaboration, GEANT4-a simulation toolkit. Nucl. Instrum. Methods Phys. Res. A **506**, 250–303 (2003). doi:10.1016/S0168-9002(03)01368-8

2. Allison, J., Amako, K., Apostolakis, J., Araujo, H., Arce Dubois, P., Asai, M., Barrand, G., Capra, R., Chauvie, S., Chytracek, R., Cirrone, G.A.P., Cooperman, G., Cosmo, G., Cuttone, G., Daquino, G.G., Donszelmann, M., Dressel, M., Folger, G., Foppiano, F., Generowicz, J., Grichine, V., Guatelli, S., Gumplinger, P., Heikkinen, A., Hrivnacova, I., Howard, A., Incerti, S., Ivanchenko, V., Johnson, T., Jones, F., Koi, T., Kokoulin, R., Kossov, M., Kurashige, H., Lara, V., Larsson, S., Lei, F., Link, O., Longo, F., Maire, M., Mantero, A., Mascialino, B., McLaren, I., Mendez Lorenzo, P., Minamimoto, K., Murakami, K., Nieminen, P., Pandola, L., Parlati, S., Peralta, L., Perl, J., Pfeiffer, A., Pia, M.G., Ribon, A., Rodrigues, P., Russo, G., Sadilov, S., Santin, G., Sasaki, T., Smith, D., Starkov, N., Tanaka, S., Tcherniaev, E., Tome, B., Trindade, A., Truscott, P., Urban, L., Verderi, M., Walkden, A., Wellisch, J.P., Williams, D.C., Wright, D., Yoshida, H.: Geant4 developments and applications. IEEE Trans. Nucl. Sci. **53**, 270–278 (2006). doi:10.1109/TNS.2006.869826
3. Allison, J., Amako, K., Apostolakis, J., Arce, P., Asai, M., Aso, T., Bagli, E., Bagulya, A., Banerjee, S., Barrand, G., Beck, B.R., Bogdanov, A.G., Brandt, D., Brown, J.M.C., Burkhardt, H., Canal, P., Cano-Ott, D., Chauvie, S., Cho, K., Cirrone, G.A.P., Cooperman, G., Cortés-Giraldo, M.A., Cosmo, G., Cuttone, G., Depaola, G., Desorgher, L., Dong, X., Dotti, A., Elvira, V.D., Folger, G., Francis, Z., Galoyan, A., Garnier, L., Gayer, M., Genser, K.L., Grichine, V.M., Guatelli, S., Guèye, P., Gumplinger, P., Howard, A.S., Hřivnáčová, I., Hwang, S., Incerti, S., Ivanchenko, A., Ivanchenko, V.N., Jones, F.W., Jun, S.Y., Kaitaniemi, P., Karakatsanis, N., Karamitrosi, M., Kelsey, M., Kimura, A., Koi, T., Kurashige, H., Lechner, A., Lee, S.B., Longo, F., Maire, M., Mancusi, D., Mantero, A., Mendoza, E., Morgan, B., Murakami, K., Nikitina, T., Pandola, L., Paprocki, P., Perl, J., Petrović, I., Pia, M.G., Pokorski, W., Quesada, J.M., Raine, M., Reis, M.A., Ribon, A., Ristić Fira, A., Romano, F., Russo, G., Santin, G., Sasaki, T., Sawkey, D., Shin, J.I., Strakovsky, I.I., Taborda, A., Tanaka, S., Tomé, B., Toshito, T., Tran, H.N., Truscott, P.R., Urban, L., Uzhinsky, V., Verbeke, J.M., Verderi, M., Wendt, B.L., Wenzel, H., Wright, D.H., Wright, D.M., Yamashita, T., Yarba, J., Yoshida, H.: Recent developments in GEANT4. Nucl. Instrum. Methods Phys. Res. A **835**, 186–225 (2016). doi:10.1016/j.nima.2016.06.125
4. Bethe, H.: Zur Theorie des Durchgangs schneller Korpuskularstrahlen durch Materie. Annalen der Physik **397**, 325–400 (1930). doi:10.1002/andp.19303970303
5. Conti, G., Mattaini, E., Santambrogio, E., Sacco, B., Cusumano, G., Citterio, O., Braeuninger, H.W., Burkert, W.: X-ray characteristics of the Italian X-Ray Astronomy Satellite (SAX) flight mirror units. In Hoover, R.B., Walker, A.B. (eds.) Advances in Multilayer and Grazing Incidence X-Ray/EUV/FUV Optics, Proc. SPIE, vol. 2279, pp. 101–109. (1994) doi:10.1117/12.193179
6. Cusumano, G., Campana, S., Romano, P., Mangano, V., Moretti, A., Abbey, A.F., Angelini, L., Beardmore, A.P., Burrows, D.N., Capalbi, M., Chincarini, G., Citterio, O., Giommi, P., Goad, M.R., Godet, O., Hartner, G.D., Hill, J.E., Kennea, J.A., La Parola, V., Mineo, T., Morris, D., Nousek, J.A., Osborne, J.P., Page, K., Pagani, C., Perri, M., Tagliaferri, G., Tamburelli, F., Wells, A.: In-flight calibration of the Swift XRT effective area. In: by Holt, S.S., Gehrels, N., Nousek, J.A. (eds.) Gamma-Ray Bursts in the Swift Era, American Institute of Physics Conference Series, vol. 836, pp. 664–667 (2006). doi:10.1063/1.2207972
7. Dayeh, M.A., Desai, M.I., Dwyer, J.R., Rassoul, H.K., Mason, G.M., Mazur, J.E.: Composition and spectral properties of the 1 AU quiet-time suprathermal ion population during solar cycle 23. Astrophys. J **693**, 1588–1600 (2009). doi:10.1088/0004-637X/693/2/1588
8. Diebold, S., Tenzer, C., Perinati, E., Santangelo, A., Freyberg, M., Friedrich, P., Jochum, J.: Soft proton scattering efficiency measurements on x-ray mirror shells. Exper. Astron. **39**, 343–365 (2015). doi:10.1007/s10686-015-9451-4

9. Dorman, B., Arnaud, K.A.: Redesign and Reimplementation of XSPEC. In: Harnden, F.R., Jr., Primini, F.A., H.E. (eds.) Astronomical Data Analysis Software and Systems X, Payne Astronomical Society of the Pacific Conference Series, vol. 238, p. 415 (2001)
10. Firsov, O.B.: Reflection of fast ions from a dense medium at glancing angles. Soviet Phys. Doklady **11**, 732 (1967)
11. Ivanchenko, V., Dondero, P., Fioretti, V., Ivantchenko, A., Lei, F., Lotti, S., Mantero, P., Mineo, T.: Geant4 simulation of protons interaction for space radiation effects. Exper. Astron. this volume (2017)
12. Jansen, F., Lumb, D., Altieri, B., Clavel, J., Ehle, M., Erd, C., Gabriel, C., Guainazzi, M., Gondoin, P., Much, R., Munoz, R., Santos, M., Schartel, N., Texier, D., Vacanti, G., XMMNewton, observatory.I.: The spacecraft and operations. Astron. Astrophys **365**, 1–6 (2001). doi:10.1051/0004-6361:20000036
13. Leccardi, A., Molendi, S.: Radial temperature profiles for a large sample of galaxy clusters observed with XMM-Newton. Astron. Astrophys **486**, 359–373 (2008). doi:10.1051/0004-6361:200809538
14. Lo, D.H., Srour, J.R.: Modeling of proton-induced CCD degradation in the Chandra X-ray observatory. IEEE Trans. Nuclear Sci. **50**, 2018–2023 (2003). doi:10.1109/TNS.2003.820735
15. Mewaldt, R.A., Cohen, C.M.S., Mason, G.M., Haggerty, D.K., Desai, M.I.: Long-term fluences of solar energetic particles from H to Fe. Space Sci. Rev. **130**, 323–328 (2007). doi:10.1007/s11214-007-9200-8
16. Remizovich, V.S., Ryazanov, M.I., Tilinin, I.S.: Energy and angular distributions of particles reflected in glancing incidence of a beam of ions on the surface of a material. Sov. J. Exper. Theor. Phys. **52**, 225 (1980)
17. Weisskopf, M.C., Brinkman, B., Canizares, C., Garmire, G., Murray, S., Van Speybroeck, L.P.: An overview of the performance and scientific results from the chandra x-ray observatory. PASP **114**, 1–24 (2002). doi:10.1086/338108